Journal of Cluster Science (2018) 29:1177–1183
https://doi.org/10.1007/s10876-018-1434-y

ORIGINAL PAPER

Synthesis, Structure and Photoluminescence Performance of a New Er^{3+}-Cluster-Based 2D Coordination Polymer

Ugur Erkarslan[1] · Adem Donmez[1,2] · Hulya Kara[1,3] · Muhittin Aygun[4] · Mustafa Burak Coban[3,5]

Received: 17 June 2018 / Published online: 27 July 2018

Abstract

A new Er^{3+}-cluster-based 2D coordination polymer with the formula $\{[Er(SSA)\cdot(H_2O)_2]\cdot(H_2O)\}_n$ (SSA = 5-sulfosalicylic acid), complex **1**, has been successfully synthesized via hydrothermal method and structurally characterized by elemental analysis, FT-IR, UV, single crystal and powder X-ray diffraction. Complex **1** reveals the Erbium atom is coordinated to eight oxygen atoms by four symmetry-related SSA ligands and two coordinated water molecules to form a distorted square-antiprismatic geometry. The photoluminescence spectrum of the complex **1** display intense pink emission with CIE chromaticity coordinates (0.540, 0.250). The complex **1** emit NIR luminescence at 1535 nm, which corresponds to the $^4I_{13/2}$–$^4I_{15/2}$ transition of Er^{3+} ion. Moreover, its full width at half maximum values is 113 nm. This complex can potentially be applied to polymeric erbium-doped optical amplifiers, planar waveguides or infrared OLEDs.

Keywords Er(III) cluster · Structure · NIR luminescence

Introduction

Recently, researchers have interest on lanthanide complexes since their particular photo-physical properties [1] and also their interesting magnetic behaviors [2–5]. Regarding their luminescent features, Ln^{3+} ions having particular properties due to their electronic configurations and energetically f-levels leads to the narrow line emission of some Ln^{3+} complexes in the near infra-red range. Preparing strong absorbing luminescent materials with Ln^{3+} ion has an importance for researchers in this respect. However, the 4f–4f transition of the Ln^{3+} ions is partially prohibited, so the absorption and photoluminescence by itself are quite small in contrast to that the luminescence lifetime is long [6–9]. This limitation forces the low absorption density of Ln^{3+} doped inorganic materials [10]. Through energy transfer, Ln^{3+} may be excited to overthrown this disadvantage by using appropriate organic ligands in their complexes. Two ways of energy transfer are that of direct coordination of an exciting multi-constituent molecule with a plurality of donor atoms, or of coordination of a simple ligand covalently linked to an excited molecule. In addition, an appropriate ligand to be designed or chosen for the formation of coordination polymers use to improve specific properties such as flexibility and versatile attachment modes [5]. The carboxylate ligands are chosen to be a perfect candidate as they constitute a good coordination with the lanthanides due to the 'hard-soft acid–base' concept. Lanthanide complexes show intense luminescence properties because the aromatic carboxylic groups are well fluorescent chromophores. Containing three potential coordination groups (–COOH, $–SO_3H$ and –OH), the 5-sulfosalicylic acid (SSA) ligand, is an important example of the multidentate O-donor ligand

Electronic supplementary material The online version of this article (https://doi.org/10.1007/s10876-018-1434-y) contains supplementary material, which is available to authorized users.

✉ Ugur Erkarslan
eugur@mu.edu.tr

[1] Molecular Nano-Materials Laboratory, Department of Physics, Faculty of Science, Mugla Sitki Kocman University, 48170 Mugla, Turkey

[2] Scientific Research Projects Coordination Unit, Mugla Sitki Kocman University, Mugla, Turkey

[3] Department of Physics, Faculty of Science and Art, Balikesir University, Balikesir, Turkey

[4] Department of Physics, Faculty of Science and Art, Dokuz Eylul University, Izmir, Turkey

[5] Center of Science and Technology Application and Research, Balikesir University, Balikesir, Turkey

and allows for the synthesis of very different complexes, exhibiting strong coordination ability. The oxygen atoms of the three different chelating groups that SSA ligand can act as hard bases being strongly coordinated to the Ln^{3+} ion acting as acids [5, 11]. Due to a good fit with the energy of the Er^{3+} ion, SSA is a highly suitable coupling ligand for Er^{3+} ions, and at the same time, the related Er^{3+} complex exhibits NIR emission.

Lanthanide complexes which show NIR-luminescence have increasingly charmed attention due to their promising applications such as medicine, biomedical analysis, laser systems, optical amplification and telecommunication networks [1, 12]. Especially, the NIR luminescence Er^{3+}-complexes is of significance because of the emission at about 1550 nm which corresponds to the spectral region used in long-distance optical fiber telecommunications [13–15]. Recently, our research group and others have been studied on the Eu^{3+}, Dy^{3+} and Tb^{3+}-based complexes emitting in the visible range [16–23], whereas the Er^{3+} containing complexes with near-infrared (NIR) luminescent properties are less developed [1, 2]. In view of the recent important progress on the structure, NIR luminescence of the Er^{3+} complexes, the synthesis and structural characterizations, and luminescent properties of a new Er(III)-cluster-based 2D coordination polymer with 5-sulfosalicylic acid (SSA) ligand is presented here.

Experimental Section

Experimental Equipment and Conditions

All purchased chemicals were provided by commercial sources and used without further purification. Elemental (C, H, N) analyses were carried out using a LECO, CHNS-932. FT-IR analysis was performed on Perkin-Elmer Spectrum 65. Solid state absorption spectra were recorded on Ocean Optics Maya 2000Pro UV–vis Spectrometer. The photoluminescence measurements were recorded using an ANDOR SR500i-BL Photoluminescence Spectrometer with Nd:YLF laser. The laser wavelength was kept constant at 349 nm and 1.3 mJ and 5 ns pulse width energy per pulse were applied to the laser source. Powder X-ray diffraction (PXRD) data were gathered using a Bruker-AXS D8-Advance diffractometer with Cu-Kα radiation (λ = 1.5418 Å).

Single crystal X-ray diffraction data were collected using a Xcalibur, Eos diffractometer with graphite monochromated Mo-Kα radiation (λ = 0.71073 Å) at 293 K. The structure was resolved by direct methods with the SHELXS program [24] and refined with full-matrix least-squares on F^2 using the SHELXL program [25] using the OLEX2 software [26]. The hydrogen atoms were positioned using idealized geometry and non-hydrogen atoms were refined anisotropically. The crystal structure of complex **1** was determined as a non-merohedral twin with the final ratio of the twin domains being 0.829(8):0.171(8). The refinement was performed with SHELXL using the data in HKLF5. During refinement of the crystal structure, we have seen the relatively high thermal parameters for some atoms (C1–C7 and O1–O8). The EADP/DFIX/DANG/SADI commands in the OLEX2 software were used to restrain the parameters of these atoms. These two factors (twin and disorder in the structure of complex **1**) could contribute for an increase in the *R*-values (R_1 = 0.11, wR_2 = 0.29) for the crystal structure of complex **1**. Detail of the supramolecular π-interactions was calculated PLATON 1.17 program [27]. Crystal data and structure refinement details are listed in Table 1. Schematic representation of the complex **1** is shown in Scheme 1.

Synthesis

$Er(NO_3)_3{\cdot}5H_2O$, (0.1 mmol) and sulfosalicylic acid (0.0254 g, 0.1 mmol) were dissolved together in 20 mL of distilled water. The pH of the mixture solution was set to 4–5 by adding NaOH solution (1 mol L^{-1}). The mixture was put into a bomb equipped with a Teflon liner (45 mL) and heated 140 °C for 5 days. After the reactant mixture was slowly cooled to the room temperature, the crystals were drawn out and cleaned using distilled water. Anal. Calcd for $C_7H_7ErO_8S{\cdot}H_2O$ (1): Calcd. C, 19.26; H, 2.08%; Found: C, 19.29; H, 2.06%, Yield: 63%.

Table 1 Crystal data and structure refinement information for complex **1**

Chemical formula	$C_7H_7ErO_8S{\cdot}H_2O$
Formula weight	436.46
Crystal system	Monoclinic
Space group	$P2_1/n$
Unit cell dimensions	a = 7.4776 (11) Å
	b = 8.8209 (14) Å β = 93.244(11)°
	c = 16.6385 (17)
V/Å^3	1095.7 (3)
Z	4
ρ_{calc}/g cm^{-3}	2.65
μ/mm^{-1}	7.89
Crystal size (mm)	0.19 × 0.14 × 0.07
Reflections collected	2041
Independent reflections	1440
Goodness–of–fit on F^2	1.05
R indices [$I > 2\sigma(I)$]	R_1 = 0.11, wR_2 = 0.29

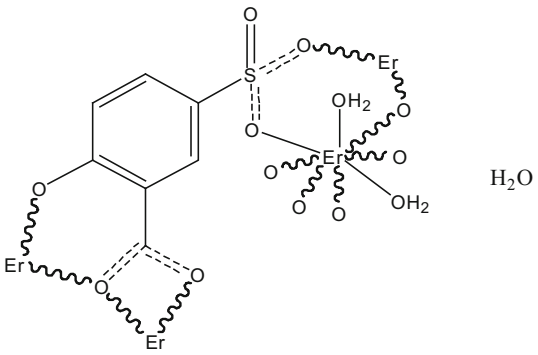

Scheme 1 Schematic representation of the polymeric complex **1**

Table 2 The selected bond lengths (Å) and bond angles (°) for complex **1**

Er1—O1	2.32 (2)	Er1—$O6^{ii}$	2.25 (2)
Er1—O2	2.37 (2)	Er1—$O7^{ii}$	2.28 (2)
Er1—O3	2.34 (2)	Er1—$O7^{iii}$	2.57 (2)
Er1—$O4^{i}$	2.32 (2)	Er1—$O8^{iii}$	2.39 (2)
O1—Er1—O2	139.9 (7)	$O6^{ii}$—Er1—O1	77.5 (7)
O1—Er1—O3	143.6 (8)	$O6^{ii}$—Er1—O2	141.5 (7)
O1—Er1—$O7^{iii}$	76.9 (7)	$O6^{ii}$—Er1—O3	79.2 (8)
O1—Er1—$O8^{iii}$	77.2 (7)	$O6^{ii}$—Er1—$O4^{i}$	121.9 (8)
O2—Er1—$O7^{iii}$	107.7 (8)	$O6^{ii}$—Er1—$O7^{iii}$	86.4 (7)
O2—Er1—$O8^{iii}$	74.9 (8)	$O6^{ii}$—Er1—$O7^{ii}$	76.3 (8)
O3—Er1—O2	71.1 (7)	$O6^{ii}$—Er1—$O8^{iii}$	136.7 (8)
O3—Er1—$O7^{iii}$	74.2 (7)	$O7^{ii}$—Er1—O1	115.6 (8)
O3—Er1—$O8^{iii}$	102.2 (8)	$O7^{ii}$—Er1—O2	77.2 (8)
$O4^{i}$—Er1—O1	73.5 (8)	$O7^{ii}$—Er1—O3	85.0 (8)
$O4^{i}$—Er1—O2	75.1 (8)	$O7^{ii}$—Er1—$O4^{i}$	72.9 (7)
$O4^{i}$—Er1—O3	142.9 (8)	$O7^{ii}$—Er1—$O7^{iii}$	155.2 (3)
$O4^{i}$—Er1—$O7^{iii}$	131.9 (7)	$O7^{ii}$—Er1—$O8^{iii}$	146.9 (7)
$O4^{i}$—Er1—$O8^{iii}$	83.0 (7)	$O8^{iii}$—Er1—$O7^{iii}$	53.8 (7)

Symmetry codes: (i) $-x+1/2$, $y-1/2$, $-z+1/2$; (ii) $-x+1$, $-y+1$, $-z+1$; (iii) $x-1/2$, $-y+3/2$, $z-1/2$

Result and Discussion

Infrared Spectroscopy

The IR spectrum of the complex **1**, as well as the spectrum of the SSA ligand, are shown in Fig. S1. The broadband observed at 3345 cm^{-1} for complex **1** is due to ν(O–H) vibration associated with the coordinated water molecule [11]. The absorption peak located at 1728–1616 cm^{-1} was absent in the spectrum of the complex. The absence of this vibration peak in the complex indicates that the SSA ligand is purified from the protons [3]. The vibration of 1603 cm^{-1} is related to ν_{as}(COO) and the peak at 1326 cm^{-1} corresponds to ν_{s}(COO) [28]. 1508 cm^{-1} is the result of the (C–C) skeleton [11]. The sulphonate group R-SO_3 leads characteristic absorption peaks of ν(S–O) vibrations in the range of 1070–1300 cm^{-1} and the ν(C–S) peaks are found in the region of 995–1070 cm^{-1} [3]. The difference of 277 cm^{-1} between asymmetric and symmetric vibration peaks of carboxyl groups in the complex **1** shows that the carboxylic groups are coordinated with the metal ion in the chelate mode [29, 30]. Moreover, the band of 644 and 988 cm^{-1} may be caused by C–H out-of-plane bending vibration of phenyl group [31].

Crystal Structure Description

Single crystal X-ray diffraction analysis shows that complex **1** crystallizes in monoclinic system with space group $P2_1/n$, forming a two-dimensional coordination polymer. The asymmetric unit of complex **1** is composed of one Er^{3+} cation, one sulfosalicylate trianion and two coordinated water molecules and one lattice water molecule. The molecular structure of complex **1**, showing the metal atom coordination environment by some atomic numbering used in the present work, is presented in Fig. 1. Each Erbium atom is coordinated to eight oxygen atoms by four symmetry-related SSA ligands and two coordinated water molecules to form a distorted square-antiprismatic geometry. The Er–O bond distances are in the range of 2.25(2)–2.57(2) Å and the O–Er–O angles are in the range of 53.8 (7)°–155.2 (3)° (Table 2). All bond distance and angles resemble in those reported earlier structures [1, 12, 32, 33]. The SSA ligand serves as μ_4-bridge to link four Erbium ions, by a bidentate chelating-bridging mode of the carboxylate, a bidentate bridging mode of the sulfonate, and a monodentate mode of the hydroxyl group. The carboxylate group is in a μ_3-η^2:η^1 bridging coordination mode: two oxygen atoms are chelating one Er^{3+} ion, and one of the oxygen atoms is bridging two Er^{3+} ions (Scheme 1).

Complex **1** is an Er^{3+}- cluster-based 2D coordination polymer and the shortest intermolecular Er…Er separations are 4.503, 8.071 and 9.858 Å in the 2D framework (Fig. 2b). The adjacent 2D frameworks are connected by O–H…O hydrogen bonds between the coordinated and lattice water molecules (Table 3). These hydrogen bonds play the key role in the construction of 3D supramolecular network (Fig. 2a). The stability of the structure of the complex **1** has been utilized by these hydrogen-bonds and π–π interactions (Fig. 3).

Prior to the spectroscopic and photoluminescence studies, a powder X-ray diffraction (PXRD) experiment has been carried out to investigate the purity of complex **1**. The PXRD results showed that the peak positions match well with those from the simulated PXRD patterns on the basis of single-crystal structure data (Fig. S2).

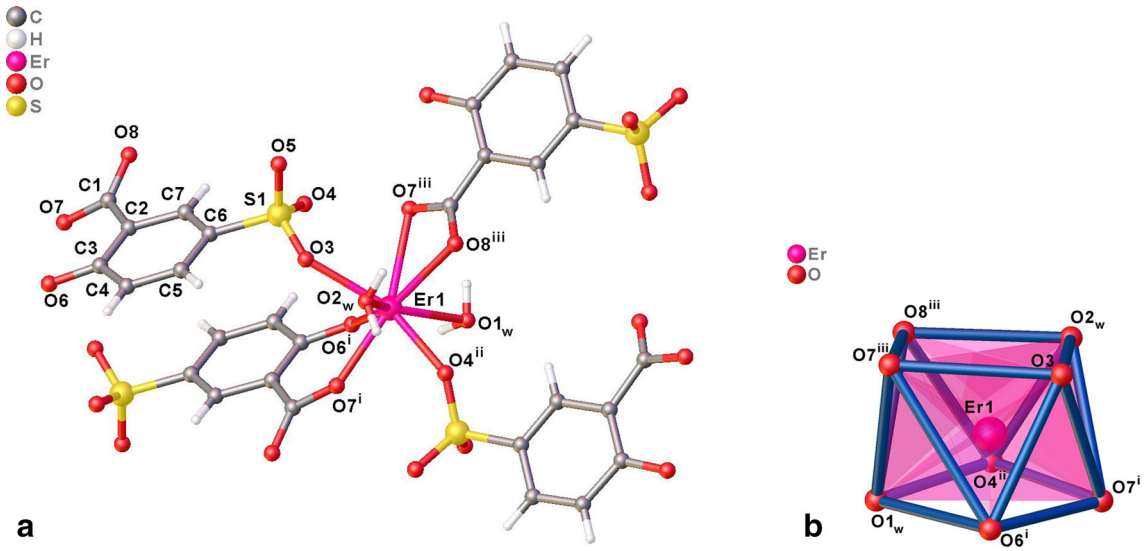

Fig. 1 **a** The molecular structure of complex **1.** Lattice water molecule is omitted for clarity. **b** The coordination environment of the Er^{3+} atom

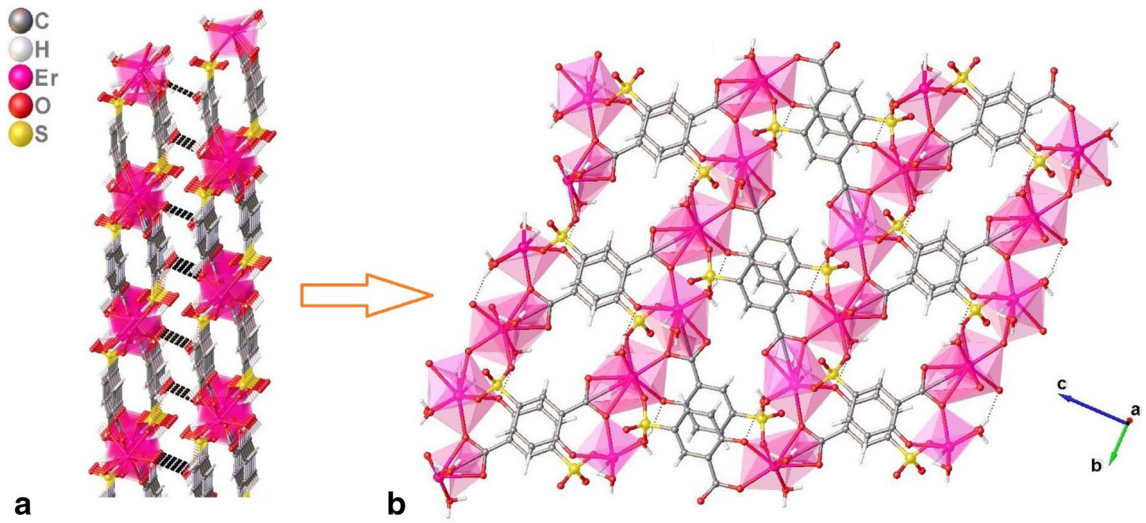

Fig. 2 **a** The hydrogen bonds interaction between adjacent clusters contributed a three-dimensional framework of complex **1**. **b** View of the two-dimensional layer of complex **1** in *ac* plane

Photo-Physical Study

The solid-state UV–Visible absorption spectra of the free ligand (SSA) and complex **1** are shown in Fig. 4. The broad absorption bands observed at λ_{max} = 307 nm and λ_{max} = 395 nm are for the ligand and at λ_{max} = 450 nm for the complex **1**, respectively. The two broad absorption bands on the spectrum for the free ligand (SSA) can be assigned to the π–π* electronic transitions from the ground-state level (S_0) to the excited level (S_1) of the ligands [22]. The broad absorption band of the complex **1** is red shifted and this shows stabilization of the ligand orbitals after complex formation [34–36].

Due to their potentially variable applications in chemical sensors and photochemistry, emissive coordination compounds are of great interest. To be able to identify the whole emission and energy-transfer process of the complex **1** and its free ligand (SSA) in the UV–visible and NIR region, the solid-state photoluminescence (PL) measurements have been taken at room temperature under the excitation at 349 nm. The emission spectrum of the free ligand (SSA) (see Fig. S3) displayed a broad navy-blue emission peak at λ_{max} = 466 nm which may be assigned to the $n \rightarrow \pi^*$ or $\pi \rightarrow \pi^*$ electronic transition (ILCT) [37–39]. The PL spectrum of the complex **1** in the visible and NIR region while it has excited at 349 nm, many characteristic emission bands for Er^{3+} ion have occurred in

Table 3 Hydrogen-bond geometry (Å, °) and the distance between ring centroids [Å] for complex **1**

D–H···A[a]	D–H	H···A	D···A	D–H···A	Symmetry
O1–H1A···O7	0.85	2.33	3.04	142	− 1/2 + x, 3/2 − y, − 1/2 + z
O1–H1A···O8	0.85	2.49	2.93	113	− 1/2 + x, 3/2 − y, − 1/2 + z
O1–H1B···O5	0.85	2.32	2.72	110	− 1 + x, y, z
O1–H1B···O6	0.85	2.19	2.85	135	1 − x, 1 − y, 1 − z
O2–H2A···O9	0.85	2.45	3.22	151	3/2 − x, 1/2 + y, 1/2 − z
O2–H2A···O8	0.85	2.55	2.89	105	− 1/2 + x, 3/2 − y, − 1/2 + z
O2–H2B···O4	0.86	2.54	2.85	103	1/2 − x, − 1/2 + y, 1/2 − z
O2–H2B···O6	0.86	1.80	2.62	158	− 1/2 + x, 1/2 − y, − 1/2 + z
O9–H9A···O8	0.85	2.19	2.96	151	x, − 1 + y, z
O9–H9B···O1	0.85	2.14	2.80	134	1/2 − x, − 1/2 + y, 1/2 − z
Cg(I)···Cg(J)			Cg···Cg		
Cg(1)···Cg(1)			3.69		1 − x, 1 − y, 1 − z
Cg(1)···Cg(1)			4.07		2 − x, 1 − y, 1 − z

[a]*D* donor, *A* acceptor, *Cg(I)* plane number I (= ring number in () above), *Cg–Cg* distance between ring centroids (Å), *Cg (1)* C2–C3–C4–C5–C6–C7

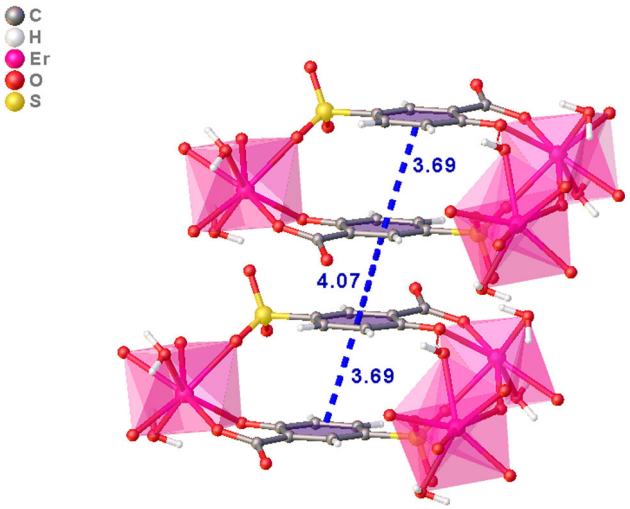

Fig. 3 π···π interaction in the complex **1**

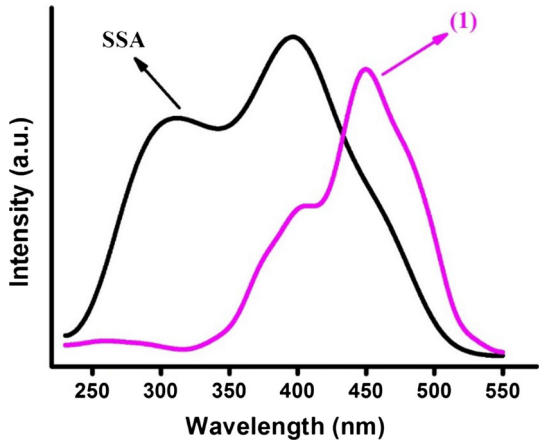

Fig. 4 The Solid state UV–Visible spectra of the ligand (SSA) and the complex **1**

both regions as indicated Fig. 5 and Fig. S4. In the UV–Vis region; five emission bands at λ_{max} = 420, 524, 550, 658 and 700 nm are attributed to the f–f transition $^4F_{5/2}\rightarrow{}^4I_{15/2}$, $^2H_{11/2}\rightarrow{}^4I_{15/2}$, $^4S_{3/2}\rightarrow{}^4I_{15/2}$, $^4F_{9/2}\rightarrow{}^4I_{15/2}$, $^4F_{7/2}\rightarrow{}^4I_{13/2}$, respectively [1, 23, 40]. In the NIR region; three emission bands at λ_{max} = 809, 1116, and 1535 nm are attribute to the f–f transition $^4I_{9/2}\rightarrow{}^4I_{15/2}$, $^4I_{11/2}\rightarrow{}^4I_{15/2}$, and $^4I_{13/2}\rightarrow{}^4I_{15/2}$, respectively [30, 41, 42]. Complex **1** shows characteristic NIR emission band centered at 1535 nm which corresponds to that the wavelength of the low-loss transmission window in telecommunication fibers [15, 43, 44]. In addition, its FWHM is 113 nm, which is much wider than the other reported Er^{3+} complexes [40, 45]. So the complex **1** would have the potential applications in the optical amplification field.

As seen in the schematic diagram for sensitization mechanism of the Er^{3+} ion by SSA ligand, lanthanide-sensitization processing consists of three steps (Fig. 6). The first step, the SSA ligand absorbs the energy and is excited to the singlet (S_1) excited state. The second step is that the energy of the (S_1) excited state is transferred to its triplet (T_1) level via intersystem crossing (ISC). In this process, the usual path for energy transfer from the SSA ligand to Er^{3+} ion causes $S_1\rightarrow T_1$ ISC from the single state to triplet state. The last step for the whole energy-transfer process is in the SSA ligand which is improved by the coordinated heavy erbium ion and subsequent energy transfer from T_1

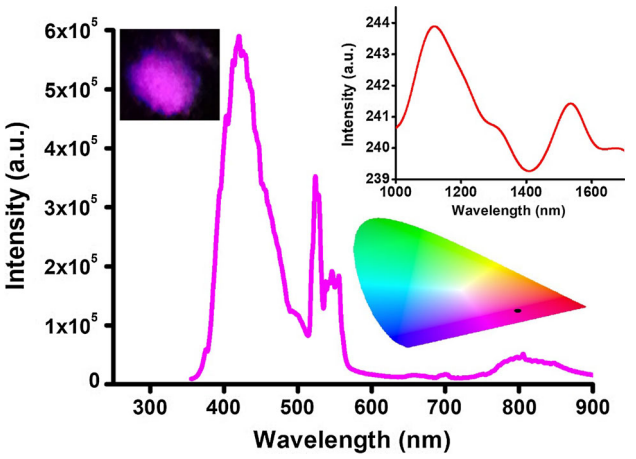

Fig. 5 Room temperature solid-state photoluminescence spectrum of the complex **1** (inset: the corresponding emission spectrum in the NIR region (1000–1700 nm). The upper-left photo is the photoluminescent image of the complex **1** while excited at 349 nm and bottom-right photo is its CIE chromaticity diagram image

to energy levels of Er^{3+} ion, resulting in the characteristic emissions of the sensitized Er^{3+} ion [32, 46].

Conclusion

We have successfully synthesized and structurally characterized by a new Er^{3+}-cluster-based 2D coordination polymer, $\{[Er(SSA)\cdot(H_2O)_2]\cdot(H_2O)\}$, complex **1**. The crystal structure and properties of the complex **1** have been studied by single-crystal X-ray diffraction and spectroscopic techniques. These studies show that each Er^{3+} atom has eight coordination and adopts a distorted square-antiprismatic geometry with four oxygen atoms from carboxylate groups, two oxygen atoms from sulfonate group and two oxygen atoms from coordinated water molecules. It may easily be concluded from the solid-state photoluminescence measurements that, utilizing sensitization processing due to strong intramolecular energy transfer from SSA ligand. The emission spectrum of the complex **1** reveals intense bright pink emission in the visible region and also typical emission of Er^{3+} in the NIR regions. As well-known effect that Er^{3+} ion, via an intra-4f shell transition from its first excited state ($^4I_{13/2}$) to the ground state ($^4I_{15/2}$), shows characteristic emission centered at 1535 nm providing that complex **1** has emission in the telecommunication wavelength standard at 1.5 μm. The complex **1** may have some potential applications like optical communication network and other technological areas.

Supplementary Material

FT-IR spectra of the ligand (SSA) and the complex **1** (Fig. S1), X-ray powder diffraction pattern of the complex **1** (Fig. S2), The solid-state photoluminescence spectrum of the ligand (SSA) (Fig. S3), the solid-state photoluminescence spectrum of the complex **1** in 600–950 nm region (Fig. S4). CCDC- 1832453 contains the supplementary crystallographic data for the complex **1**. This data can be obtained free of charge from The Cambridge

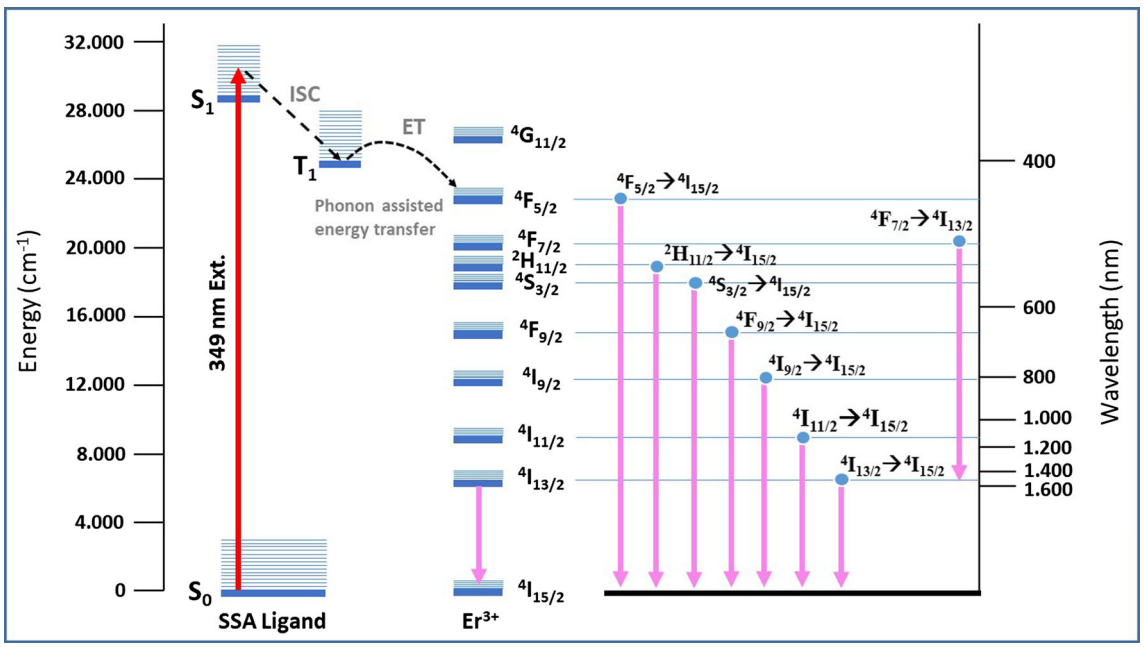

Fig. 6 Schematic diagram for sensitization mechanism of the Er^{3+} ion by SSA ligand

Crystallographic Data Center Via http://www.ccdc.cam.ac.uk/data_request/cif.

Acknowledgements The authors are grateful to the Research Funds of Mugla Sitki Kocman University (BAP-2016/52) for the financial support, Dokuz Eylul University for the use of the Agilent Xcalibur Eos diffractometer (purchased under University Research Grant No. 2010.KB.FEN.13) and Balikesir University, Science and Technology Application and Research Center (BUBTAM) for the use of the Photoluminescence Spectrometer.

References

1. P. Martín-Ramos, M. D. Miranda, M. R. Silva, M. E. S. Eusebio, V. Lavín, and J. Martín-Gil (2013). *Polyhedron.* **65**, 187.
2. H.-Y. Shen, W.-M. Wang, H.-L. Gao, and J.-Z. Cui (2016). *RSC Adv.* **6**, 34165.
3. X. Li, Y. Lu, Y. Bing, and M. Q. Zha (2012). *Synth. React. Inorg. Met. Nano-Met. Chem.* **42**, 698.
4. S. Alghool, M. S. Zoromba, and H. F. A. El-Halim (2013). *J. Rare Earths.* **31**, 715.
5. R. S. Zhou, L. Ye, H. Ding, J. F. Song, X. Y. Xu, and J. Q. Xu (2008). *J. Solid State Chem.* **181**, 567.
6. B. Ay, E. Yildiz, and İ. Kani (2018). *Polyhedron.* **142**, 1.
7. Z. Hnatejko, A. Kłonkowski, S. Lis, K. Czarnobaj, M. Pietraszkiewicz, and M. Elbanowski (2000). *Mol. Cryst. Liq. Cryst. Sci. Technol. Sect. A Mol. Cryst. Liq. Cryst.* **354**, 207.
8. M. Kawa and J. M. J. Fréchet (1998). *Chem. Mater.* **10**, 286.
9. C. Piguet, A. F. Williams, J. C. G. Bünzli, G. Bernardinelli, and G. Hopfgartner (1993). *J. Am. Chem. Soc.* **115**, 8197.
10. S. I. Klink, H. Keizer, and F. C. J. M. van Veggel (2000). *Angew. Chemie.* **39**, 4319.
11. Z. Lu, L. Wen, J. Yao, H. Zhu, and Q. Meng (2006). *CrystEngComm.* **8**, 847.
12. Z. Ahmed, R. E. Aderne, J. Kai, J. A. L. C. Resende, H. I. Padilla-Chavarría, and M. Cremona (2017). *RSC Adv.* **7**, 18239.
13. A. Mech, A. Monguzzi, F. Meinardi, J. Mezyk, G. Macchi, and R. Tubino (2010). *J. Am. Chem. Soc.* **132**, 4574.
14. S. Penna, A. Reale, R. Pizzoferrato, G. M. Tosi Beleffi, D. Musella, and W. P. Gillin (2007). *Appl. Phys. Lett.* **91**, 021106.
15. A. Polman (1997). *J. Appl. Phys.* **82**, 1.
16. M. B. Coban (2018). *J. Mol. Struct.* **1162**, 109.
17. M. B. Coban, C. Kocak, H. Kara, M. Aygun, and A. Amjad (2017). *Mol. Cryst. Liq. Cryst.* **648**, 202.
18. G. Oylumluoglu (2018). *J. Clust. Sci.* **29**, 649.
19. G. Oylumluoglu, M. B. Coban, C. Kocak, M. Aygun, and H. Kara (2017). *J. Mol. Struct.* **1146**, 356.
20. M. B. Coban, A. Amjad, M. Aygun, and H. Kara (2017). *Inorg. Chim. Acta.* **455**, 25.
21. J. P. Leonard and T. Gunnlaugsson (2005). *J. Fluoresc.* **15**, 585.
22. X. Zhou, X. Zhao, Y. Wang, B. Wu, J. Shen, L. Li, and Q. Li (2014). *Inorg. Chem.* **53**, 12275.
23. M. B. Coban (2017). *J. Balıkesir Inst. Sci. Technol.* **19**, 7.
24. G. M. Sheldrick (2008). *Acta Crystallogr. Sect. A Found. Crystallogr.* **64**, 112.
25. G. M. Sheldrick (2015). *Acta Crystallogr. Sect. C Struct. Chem.* **71**, 3.
26. O. V. Dolomanov, L. J. Bourhis, R. J. Gildea, J. A. K. Howard, and H. Puschmann (2009). *J. Appl. Crystallogr.* **42**, 339.
27. A. L. Spek (2009). *Acta Crystallogr. Sect. D Biol. Crystallogr.* **65**, 148.
28. X. Q. Wang, M. X. Li, X. He, M. Shao, and Z. X. Wang (2015). *Inorg. Chim. Acta.* **427**, 273.
29. M. B. Coban, U. Erkarslan, G. Oylumluoglu, M. Aygun, and H. Kara (2016). *Inorg. Chim. Acta.* **447**, 87.
30. S. Destri, M. Pasini, W. Porzio, F. Rizzo, G. Dellepiane, M. Ottonelli, G. Musso, F. Meinardi, and L. Veltri (2007). *J. Lumin.* **127**, 601.
31. N. Chen, M. X. Li, P. Yang, X. He, M. Shao, and S. R. Zhu (2013). *Cryst. Growth Des.* **13**, 2650.
32. Q. Zhong, H. Wang, G. Qian, Z. Wang, J. Zhang, J. Qiu, and M. Wang (2006). *Inorg. Chem.* **45**, 4537.
33. P. Martín-Ramos, P. S. P. Silva, P. Chamorro-Posada, M. R. Silva, B. F. Milne, F. Nogueira, and J. Martín-Gil (2015). *J. Lumin.* **162**, 41.
34. E. Gungor, M. B. Coban, H. Kara, and Y. Acar (2018). *J. Clust. Sci.* **2**, 38.
35. M. B. Coban, E. Gungor, H. Kara, U. Baisch, and Y. Acar (2018). *J. Mol. Struct.* **1154**, 579.
36. E. Gungor, M. B. Coban, H. Kara, and Y. Acar (2018). *J. Clust. Sci.* **29**, 533.
37. S. Yoopensuk, P. Tongying, K. Hansongnern, C. Pakawatchai, S. Saithong, Y. Tantirungrotechai, and N. Leesakul (2012). *Spectrochim. Acta Part A Mol. Biomol. Spectrosc.* **86**, 538.
38. E. Otgonbaatar, M.-C. Chung, K. Umakoshi, and C.-H. Kwak (2015). *J. Nanosci. Nanotechnol.* **15**, 1389.
39. S. Chooset, A. Kantacha, K. Chainok, and S. Wongnawa (2018). *Inorg. Chim. Acta.* **471**, 493.
40. X. Sun, B. Li, L. Song, J. Gong, and L. Zhang (2010). *J. Lumin.* **130**, 1343.
41. P. Martín-Ramos, P. Chamorro-Posada, M. Ramos Silva, P. S. Pereira Da Silva, I. R. Martín, F. Lahoz, V. Lavín, and J. Martín-Gil (2015). *Opt. Mater. (Amst).* **41**, 139.
42. Q. Sun, P. Yan, W. Niu, W. Chu, X. Yao, G. An, and G. Li (2015). *RSC Adv.* **5**, 65856.
43. S. Sarkar, V. N. K. B. Adusumalli, and V. Mahalingam (2015). *Capobianco JA* **17**, 17577.
44. H. Wang, G. Qian, Z. Wang, J. Zhang, Y. Luo, and M. Wang (2005). *J. Lumin.* **113**, 214.
45. D. Liu, C. Li, Y. Xu, D. Zhou, H. Wang, P. Sun, and H. Jiang (2017). *Polym. (U. K.)* **113**, 274.
46. H. Reiss and A. Heller (1985). *J. Phys. Chem.* **89**, 4207.